Transactions on Energy Systems and Engineering Applications

Article

Triboelectric nanogenerator to harness energy from low-frequency and low-amplitude vibrating sources

Om Prakash Prabhakar[1], Dhananjay Sahu[1] and Raj Kumar Sahu[1,*]

[1] Department of Mechanical Engineering, National Institute of Technology Raipur, Chhattisgarh - 492010, India.
[*] Correspondence: raj.mit.mech@gmail.com

Received: 02 April 2024; Accepted: 07 September 2024; Published: 04 March 2025

Abstract: Dielectric Elastomer Generator (DEG) stands out as a promising electromechanical device to harness energy from non-conventional sources owing to its ability to convert mechanical energy into electrical power. DEG with no rotating part demonstrates a high performance-to-weight ratio with ease in fabrication and compactness that sets it apart from traditional energy harvesting techniques. Triboelectric nanogenerators (TENGs) belong to a self-powered class of DEG that capitalizes on low-frequency and amplitude mechanical sources. Existing models for predicting the performance of TENGs often assume parameters such as frequency, amplitude, and relative permittivity are constant. However, these parameters can vary depending on the specific application. In this study, a modified model is proposed to comprehensively investigate the performance of TENG in real-world conditions considering fluctuations in frequency, amplitude, and varying relative permittivity of elastomer layers. Results indicate that at a higher frequency of 55 Hz, there is a significant increase in output voltage, attributed to the higher energy release rate due to increased velocity. The study also emphasizes the role of the relative permittivity of TENG layers, revealing that elastomer layers with higher dielectric constants generate more voltage and power (151%) compared to those with lower values, particularly at a separation distance of 0.1mm. The findings of this study exhibit notable concurrence with previously reported values and offer a valuable framework for researchers seeking to tailor energy generators for enhanced performance and precision for harnessing energy from low-frequency and low-amplitude sources.

1. Introduction

To reduce the use of non-renewable energy and increase the share of green energy in day-to-day life, researchers have demonstrated several methods over the years [1]. Progress in technology has provided a new path to harness the energy from non-conventional energy sources and thus increase green energy. To convert energy directly from mechanical to electricity, piezoelectric [2, 3], electromagnetic [4, 5],

How to cite this article: Om Prakash Prabhakar; Dhananjay Sahu; Raj Kumar Sahu. Triboelectric nanogenerator to harness energy from low-frequency and low-amplitude vibrating sources. *Transactions on Energy Systems and Engineering Applications*, 6(1): 669, 2025. DOI:10.32397/tesea.vol6.n1.669

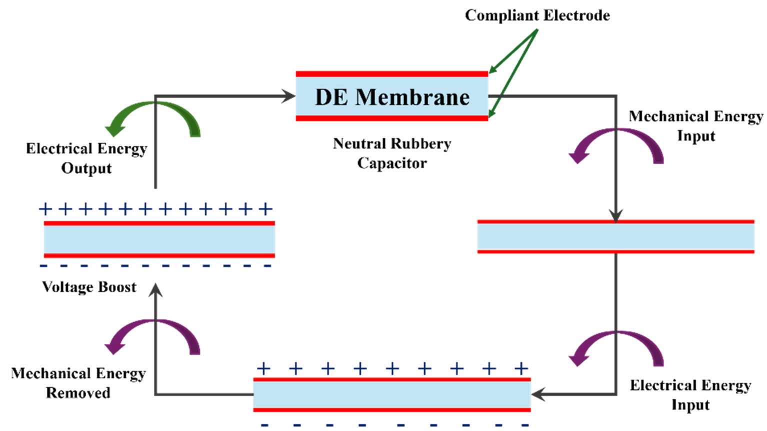

Figure 1. Schematic representation of different stages in dielectric elastomer generators [16].

electrostatic [6,7], triboelectric [8,9], energy generators have been assessed for different energy sources in last decades [10–15].

Electrostatic and triboelectric energy generators are promising due to the lack of rotating components which makes them light in weight and compact [16]. The electrostatic principle used for energy extraction using Dielectric Elastomer Generator (DEG) consists of an elastomeric membrane layered with compliant electrodes on each surface and works as a rubbery capacitor. Energy conversion (mechanical to electrical) takes place with two voltages and a mechanical source in four stages [17–19]. First, the undeformed and electrically neutral rubber capacitor is stretched by an external mechanical force to get deformed and store strain energy as shown in Figure 1. In the second stage, an external voltage is supplied to the deformed membrane due to which an additional charge accumulates on each side of the surface (compliant electrodes). In the third stage, mechanical force is removed and due to elasticity, it starts to regain its original size and shape, and charge density gets increased in a particular area. In the fourth stage, increased charge density is extracted as electrical energy as $V_{output} > V_{input}$. Overall, the electrostatic force and charge are responsible for the energy conversion, therefore the mechanism also termed as an electrostatic energy generator.

Although DEG can be employed to harness energy, each cycle needs one voltage input V_{input}. In this context, the integration of self-powered triboelectric nanogenerators (TENG), appears to be a promising alternative to address these limitations of DEG [20]. TENG has emerged as a notable innovation, adept at converting ambient mechanical energy into scalable electrical output. These devices have gained attention as a compelling alternative to existing power solutions for self-powered tactile and sensing device integration [21]. To harvest energy from the ambient sources, electrostatic mechanism-based nanogenerators piezoelectric nanogenerators (PENG) [22] and triboelectric nanogenerators (TENG) reported by the researchers [8,23–25]. PENG is a nanowire-based energy harvester in which nanowires of ZnO is used to harness energy instead of dielectric elastomer used in TENG. Though, the power generated from nano-generators are low as compared to DEGs, the self-powering capacity (no input voltage) adds an extra edge to the PENG/TENG.

The setup of a triboelectric nanogenerator is a type of laminated structure. It consists of a lower electrode on which dielectric elastomer acts as a medium then some other material or air and finally a top electrode. The major components of TENG are dielectric elastomer and complaint electrodes [26]. This system resembles with parallel plate capacitor system in which two electrodes act as two parallel plates and dielectric elastomer and air act as slabs of two mediums (Figure 2). TENG can operate in three

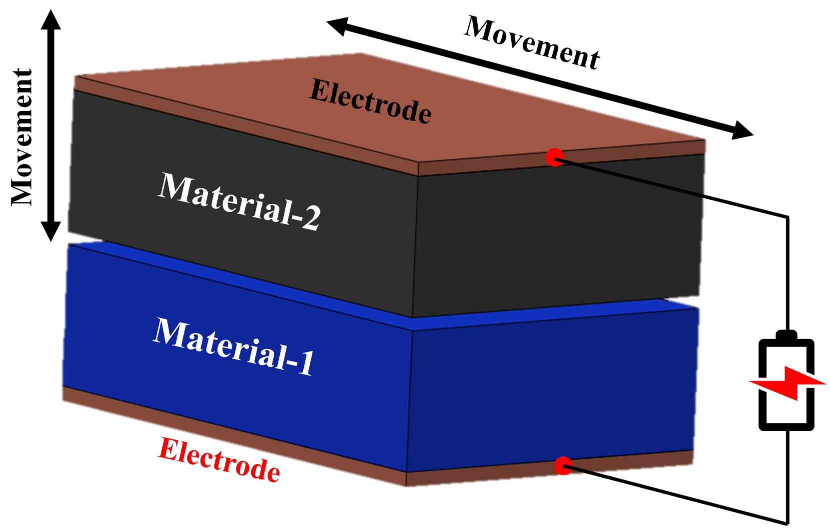

Figure 2. Schematic representation of different stages in dielectric elastomer generators[16].

configurations, first when, one electrode is kept fixed while the other electrode along with the DE layer moves towards the fixed layer through an air/dielectric elastomer layer (separation mode) [27]. In the second configuration where the moving electrodes are just in contact with the upper DE or electrode layer (contact mode), in this case, there is no additional mechanical force on the moving DE layer. Lastly when the external mechanical energy force compresses the moving layers between the electrodes (compression mode). In this study, the investigation was focused on the separation type of TENG.

Unlike electromagnetic generators which operate at high frequencies, triboelectric nanogenerators (TENGs) work at low frequencies [8]. There is an abundance of low-frequency mechanical energy around, such as vibration, wind, water waves etc to use as the input source to the TENG. These low-frequency motions cannot be harvested effectively using electromagnetic or electrostatic generators. This problem can be overcome by using TENG. Because of its simple structure, ease of fabrication and high efficiency, TENG can replace the battery in low-power electronic devices. Also, the self-powering nature of TENG adds an advantage over the DEG. The concept of a self-powering system has been demonstrated by many researchers in recent years [22, 28–31]. To utilize the low-frequency energy as an input for the TENG, wang et al. [8] developed a spherical energy generator of 6 cm and used water wave of 1.43 Hz and reported an output current of $1\mu A$. Behera et al. [32] investigate the self-powered TENG for traffic monitoring operated at low frequency of 2 Hz and reported the peak voltage of 17.8 V and current of 190 nA. In an another study Quang et al. [9] used bidirectional air with wind velocity range of 9.2-18.4 $\frac{m}{s}$ and higher frequency $(> 100Hz)$ as an input energy source and reported higher current output $(> 50\mu A)$. In a recent study on TENG Wardhana et al. [27], developed a contact-separation-compression type energy harvester and used an energy input with an amplitude of 0.2-0.9mm and frequency variation of 1-30Hz and reported output voltage was in the range of 0.2-2V.

In the prior TENG model, the assessed frequency range was either below 30Hz or exceeding 100Hz. Yet, typical mechanical systems vibrate within the 10-100Hz range, as seen in household energy generators and lathes [33]. Also, the effect of induced strain on dielectric permittivity was held constant, although it does vary with strain [34]. Babu et al. [35] and Hajra et al. [36] investigated the various frameworks for TENG from a materials perspective and reported that the performance possesses a significant impact based on the materials used in the fabrication. To devise an efficient TENG suitable for low-amplitude and low-frequency vibrating sources, a comprehensive understanding of various parameters is essential. In this study, we introduce a tailored model to predict the performance of contact-separation-compression type TENG within real-world settings. This model encompasses variations in frequency, amplitude, and relative permittivity within the separation mode. The outcomes derived from this adapted model are observed in good agreement with existing research while showcasing an enhanced voltage output. The modified model is expected to assist researchers to fabricate or adapt TENG systems for enhanced performance across a spectrum of vibrating energy sources.

2. Constitutive Model

For a single layer dielectric elastomer-based contact-separation-compression TENG (Error! Reference source not found.), with an entrapped air and DE thickness of δ and d_1 respectively, negligible thickness of compliant electrodes under the influence of an external electric field (E), the potential drop across the electrodes can be written as,

$$\Delta V = Ed, \tag{1}$$

$$D = \epsilon E = \sigma, \tag{2}$$

where, d is the total distance between the two electrodes (i.e., $d = d_{DE} + d_a$ for separation mode), ϕ is dielectric flux and σ is charge density. The charge accumulated on the electrodes with an area A can be calculated in terms of charge density (σ) as,

$$Q = \sigma A = \phi A. \tag{3}$$

By using Equations (1) to (3), voltage drop can be rewritten,

$$\Delta V = \frac{\sigma}{\epsilon} d. \tag{4}$$

In the separation mode, the resulting electrical potential difference can be expressed in terms of voltage drop in air (ΔV_1) and DE (ΔV_2) layer,

$$\Delta V = \Delta V_1 + \Delta V_2, \tag{5}$$

$$\Delta V = \frac{\phi}{\epsilon_0}\delta + \frac{\phi}{\epsilon_0 \epsilon_r} d_1, \tag{6}$$

$$\Delta V = \left(\delta + \frac{d_1}{\epsilon_r}\right)\frac{\phi}{\epsilon_0}, \tag{7}$$

while the capacitance of the combined layered system,

$$C = \frac{Q}{\Delta V} \tag{8}$$

$$C = \frac{Q}{\left(\delta + \frac{d_1}{\epsilon_r}\right)\frac{\phi}{\epsilon_0}} \tag{9}$$

$$C = \frac{\epsilon_0 A}{\left(\delta + \frac{d_1}{\epsilon_r}\right)} \tag{10}$$

In contact mode, (Figure 2) the dielectric elastomer (Material-1 and 2) layer will be in direct contact with the upper electrode so, $\delta = 0$, the capacitance in this condition can be calculated by,

$$C = \frac{\epsilon_0 A}{\left(\frac{d_1}{\epsilon_r}\right)} = \frac{\epsilon_r \epsilon_0 A}{d_1}, \tag{11}$$

whereas, in compression mode, the thickness of dielectric elastomer is less than the original thickness and the capacitance can be represented by Equation (7), only the value will change in compression mode. Here, Kirchhoff's law and Ohm's law for the above-discussed layer system are defined as follows:

$$V_R + V_{ma} = 0, \tag{12}$$

$$V_R = Ri, \tag{13}$$

$$i = i_{ma}, \tag{14}$$

$$q_{ma} = K_{ma} C_{ma} V_{ma}, \tag{15}$$

where R is the internal resistance of the data logger, the subscript ma refers to a capacitor consisting of air and dielectric elastomer, K is the interaction coefficient and the suffix ma represents the interaction between the air layer and the dielectric elastomer and depends on $d\delta/dt$ before contact as follows:

$$K_{ma} = K_f \frac{d\delta}{dt} = K_f \frac{d}{dt}\{d(x)\} = \frac{d}{dt}\{(1 - \cos 2\pi f_v t) A_v\}, \tag{16}$$

where, A_v is the separation amplitude, f_v is the vibration frequency, and K_f is the electrification coefficient considering the experimental conditions. Then, the following equations can be finally derived:

$$V_R = -V_{ma}, \tag{17}$$

$$Ri = -\frac{q_{ma}}{K_{ma} C_{ma}}, \tag{18}$$

$$i = \frac{dq}{dt} = \frac{dq_{ma}}{dt}, \tag{19}$$

$$\frac{dq_{ma}}{dt} = -\frac{q_{ma}}{R K_{ma} C_{ma}}. \tag{20}$$

3. Results and discussion

The lower dielectric layer is separated by a thin layer of air (separation mode). The lower electrode moves upward and ultimately first meets the upper electrode (contact mode) and then compression (compression mode) of the DE layers takes place. The performance of TENG greatly depends on the movement of the lower DE layer (velocity). Separation velocity at different frequencies of energy input shows a similar movement pattern as depicted in Figure 3 with with slight improvement as compared to the lower frequency. Variation in frequency affects the phase of the vibration, which shows very low impact on the maximum velocity. For further investigation, the frequency of 55 Hz is considered from all tested frequencies, as it reaches maximum velocity in a time frame comparable to that of the existing model.

In a previous study [27], the frequency was kept between 10-30 Hz. Whereas mechanical devices vibrate with a frequency between 10-100 Hz and with lower amplitude (in range of few mm). In present

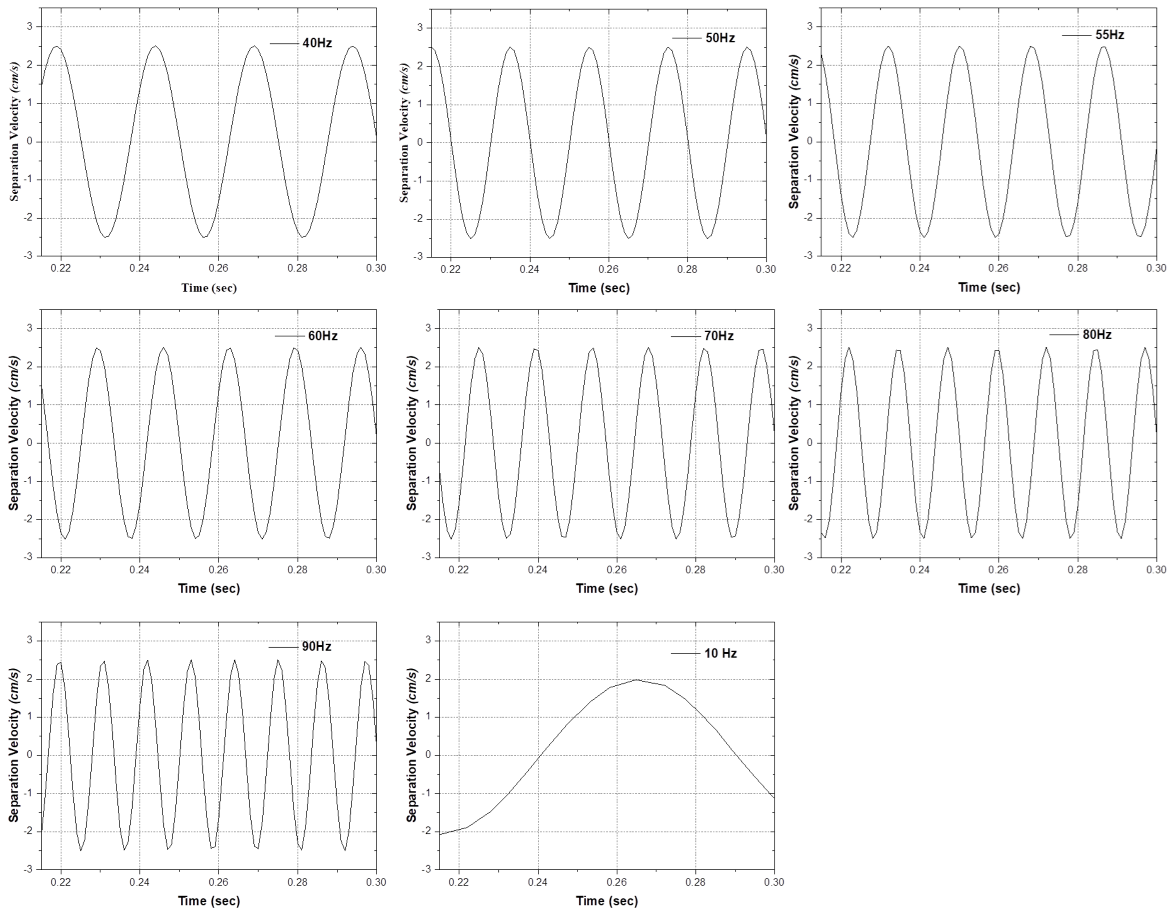

Figure 3. Separation velocity of lower dielectric elastomer layer on different frequencies.

work a single frequency of 55 Hz with a similar amplitude $(0.2mm)$ of energy source to TENG is being considered for the calculation purpose. The modified model gives higher velocity as compared to the existing model Figure 4. The possible reason for higher velocity may be due to the higher frequency of the input energy source as for any vibrating energy source, the velocity is the function of amplitude, frequency, and time.

For TENG, generators the output voltage (V) is another essential aspect and it should be as high as possible. The result of the modified model (Figure 5(a)) for TENG provides higher voltage output with the same amplitude of energy source as compared to the existing model for dielectric elastomer generator. The possible reason for such behaviour may be, the increased velocity of the DE layer. At higher amplitude and frequency, the gap between the electrodes reduces faster than the lower values of the same data, which provides less time to release energy from the rubbery-like capacitor structure of the TENG. The percentage enhancement in the voltage is quite significant in Figure 5(b), the rate at lower amplitude is higher than the higher value. For the same amplitude and low frequency modified TENG model gives more output voltage than the contact type usual dielectric elastomer generator [37]. However, design parameters (material selection, entrapped medium, etc.) also affect the performance of TENG. In the next step, a simulation study of the selected material effect on the performance of TENG is being carried out.

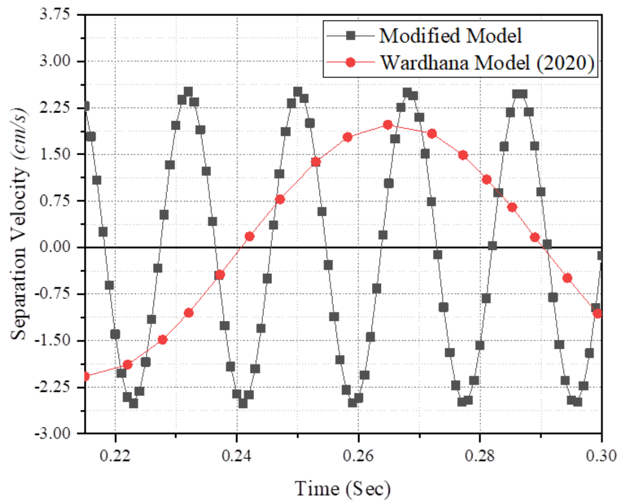

Figure 4. Schematic representation of different stages in dielectric elastomer generators[16].

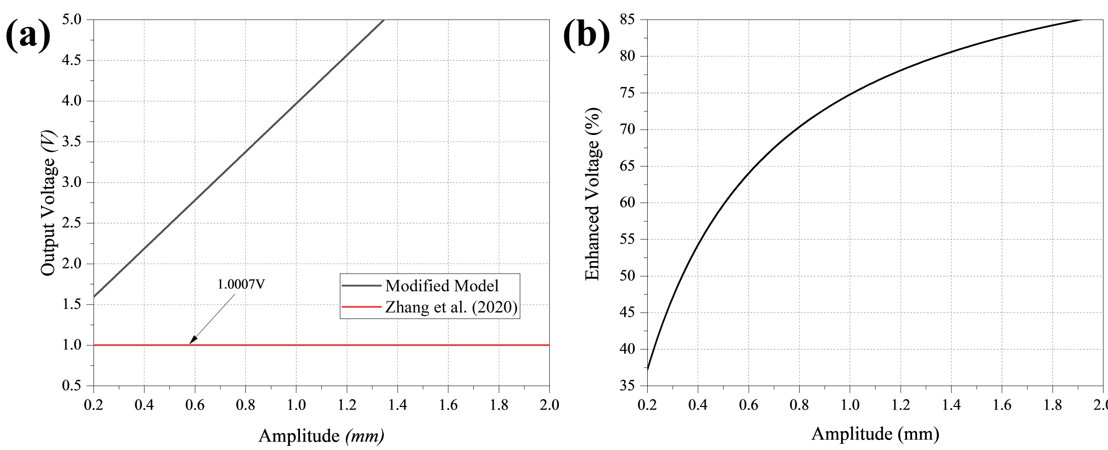

Figure 5. (a) The variation of voltage in triboelectric nanogenerator (TENG) at 55 Hz for modified model and existing model [15] (b) Enhanced output voltage at various amplitude of input energy source of constant frequency (55 Hz) as compared to 10 Hz frequency.

For material and design analysis of the Triboelectric Nanogenerator (TENG), we employed COMSOL Multiphysics with electrostatic and stationary study conditions in a 2D study setup. The TENG design maintained small, consistent dimensions for each dielectric elastomer layer $(30mm \times 0.22mm)$, with the surrounding medium's relative permittivity (RP) set at 1. We designated the outer box layer as an infinite domain, grounding it, while one dielectric elastomer layer received a unique ground voltage of 0V. Uniform surface charge density was applied to each layer to maintain overall charge neutrality. The initial electrode state featured a floating potential with distinct positive and negative charges. Subsequently, we conducted a parametric analysis, adhering to the previously outlined amplitude specifications. From the result, (Figures 6 and 7) it is quite evident that the two layers accumulate different amounts of voltage. For an instance with a separation distance (δ) between the layer was 0.1mm the maximum positive voltage of 3.29V accumulated on the upper layer of the TENG while the negative voltage was lower $(3.1V)$.

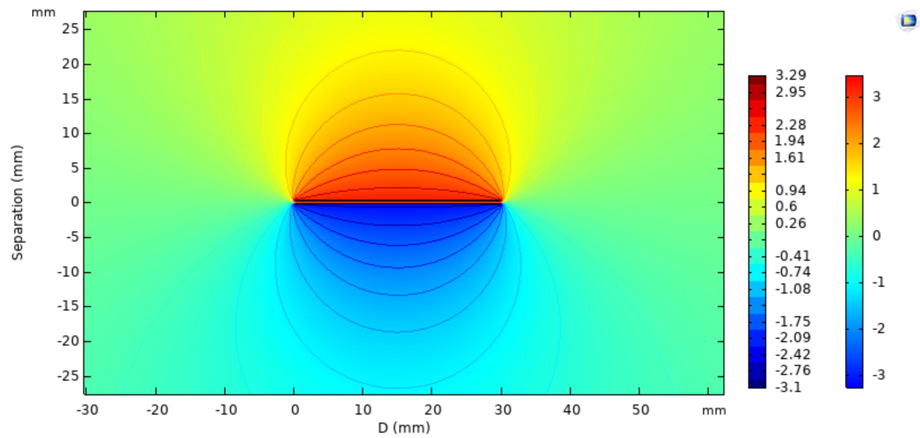

Figure 6. Voltage output for Silicone-VHB pair of dielectric elastomers at a separation distance of 0.1mm.

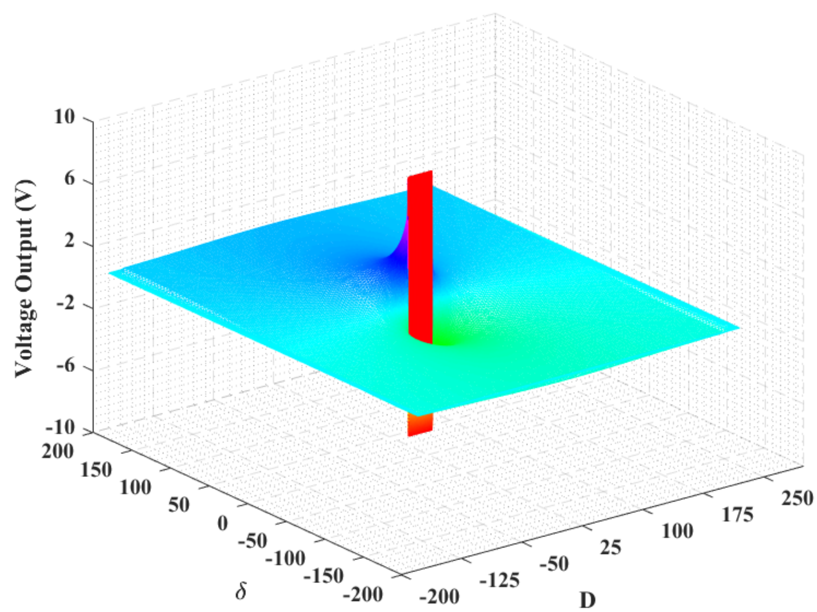

Figure 7. Voltage distribution on the two surfaces of the TENG in the case of Silicone and VHB.

The possible reason for the different accumulated charge on layers may be the difference in the relative permittivity of the silicone $(\varepsilon_r = 11.7)$ and VHB $(\varepsilon_r = 4.7)$ Figure 2. Whereas the voltage distribution along the width (D) of layer was constant.

Further to investigate the influence of the material pair on the performance of TENG, two commercially available dielectric elastomers Elastosil and silicone were considered. Figure 8 shows the voltage output at a separation distance of 0.1mm the positive accumulated charge on the upper surface (3.029V) while negative charge on lower layer (3.021V). The maximum accumulated charge is lesser as compared to the previous pair of the material (Silicone-VHB). A slightly higher difference in the relative permittivity of the material may be the reason for such output behaviour of the TENG with Elastosil-Silicone pair of dielectric elastomers. Figure 9 shows the distribution of charge inside the box along the width and the separation of the DE layers. Voltage density decreases with both distances from the layers.

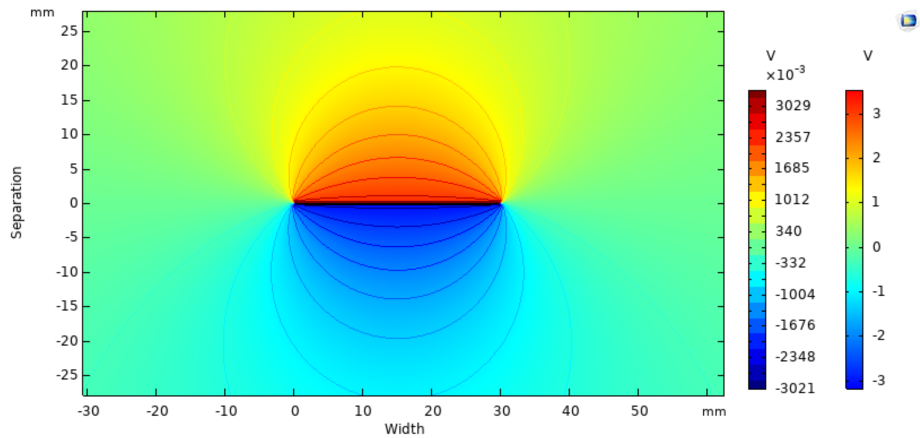

Figure 8. Voltage output for Elastosil-Silicone pair of dielectric elastomers.

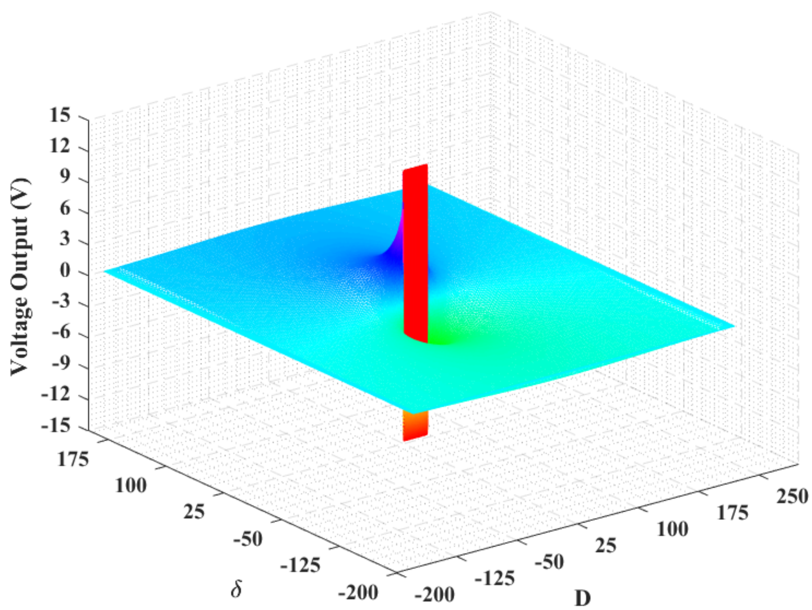

Figure 9. Voltage distribution on each side of the dielectric elastomer layer.

In the next step, the Elastosil-VHB material was selected to minimize the gap between relative permittivity between the two layers. Figure 10 shows the negative and positive distribution of the voltage on both layers. The upper layer accumulates the positive charge of 7.2V while lower that of -7.84V, which is higher than as compared to previous two conditions. It is evident from the result, that with the closer gap in relative permittivity, the maximum voltage accumulation increases significantly in similar conditions. Figure 11 shows the voltage distribution in the space around the DE layer in TENG. In all three pair materials, the lower layer of DE was moving while keeping the upper fixed [38].

Figure 12 shows the comparison between the considered pairs of DE layers to study the performance of TENG output performance. The output voltage (V_{out}) increases with the increase in separation distance and indicates a higher amplitude energy input requirement to generate the deformation in the layer. A

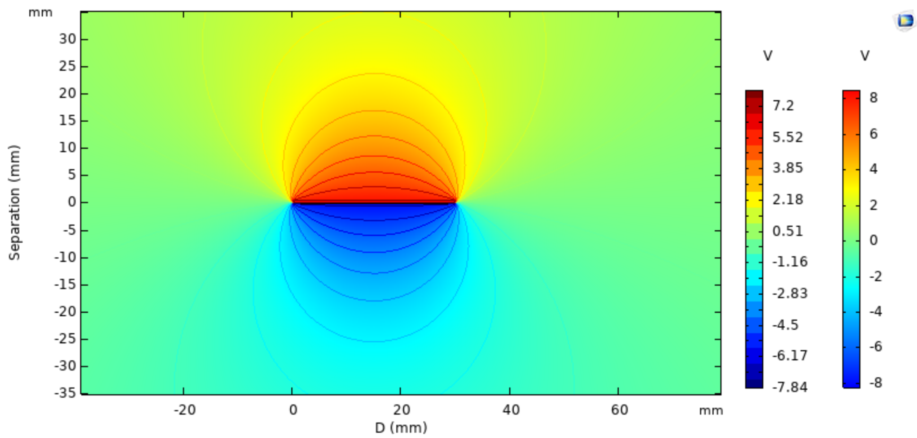

Figure 10. Voltage accumulation on different dielectric elastomer (DE) layers (Elastosil-VHB).

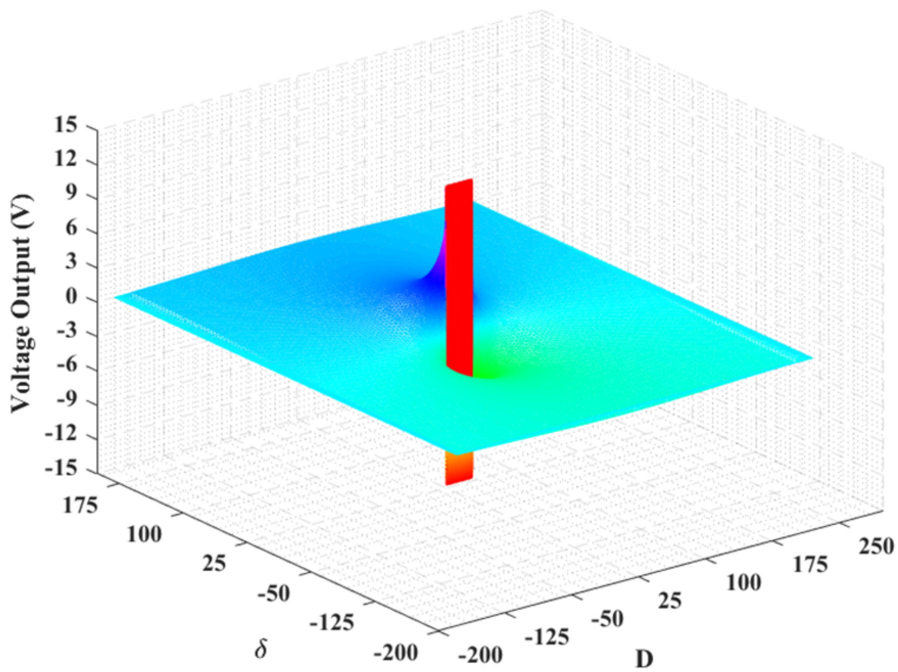

Figure 11. Voltage distribution with gap and along the length of the DE layers in the case of Elastosil-VHB.

general household vibrating machine has amplitude in the range of a fraction of mm, so the considered separation distance was kept 0.1mm [33].

Further, the electrical energy stored in the TENG system was investigated. Figure 14 shows the variation in the amount of total electrical energy stored with the phase angle of the vibrating source. In Elastosil-VHB and Silicone-VHB pairs the amount of stored energy is the same, while for Elastosil-Silicone it is higher. The possible reason for the difference in stored energy may be the permittivity of the moving layer. In the first case of lower energy, the moving layer was VHB while in the higher condition, it was Silicone [37].

The varying energy outputs (0.0390 μ W for Elastosil-silicone, 0.0976 μ W for Elastosil-VHB, and 0.0388 μ W for silicone-VHB) in TENG arise from differences in triboelectric properties and mechanical interactions of the materials. Elastosil and silicone, being similar in triboelectric behaviour, yield a modest energy output, whereas Elastosil paired with VHB, which has contrasting triboelectric characteristics,

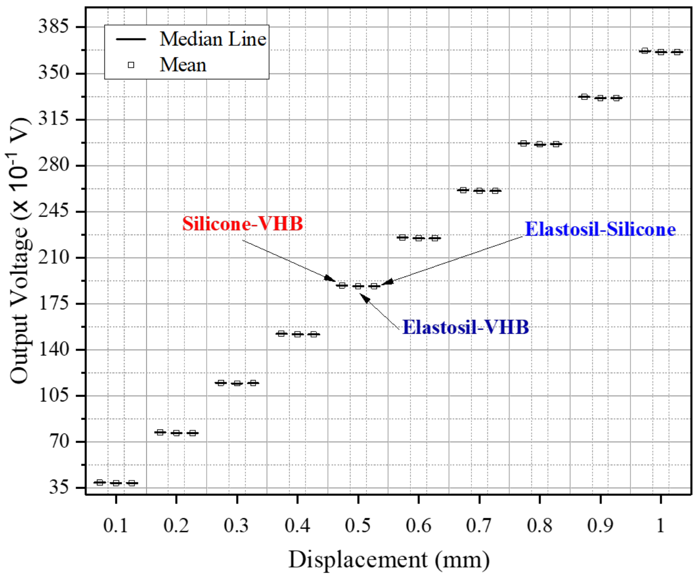

Figure 12. Maximum voltage accumulated on the layers of the DE at different separation distances.

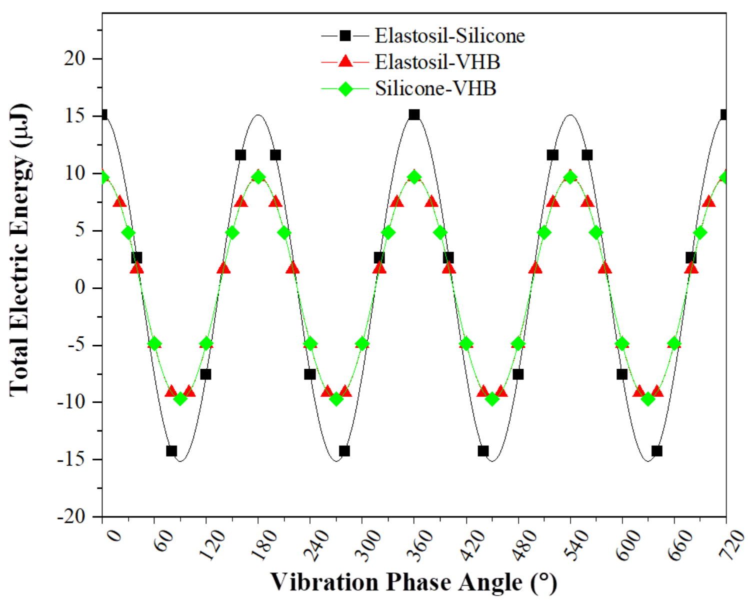

Figure 13. Total electrical energy stored in TENG with the phase of vibrating source for different pairs of material.

exhibits higher energy generation due to enhanced charge transfer efficiency [39–41]. Additionally, the results align with Yadava et al. [42], supporting the statement that electronic devices require a high dielectric constant and low losses. The lower output of the silicone-VHB combination can be attributed to less effective contact and charge separation mechanisms influenced by material compatibility and surface conditions. The energy conversion efficiencies of 24.69%, 70.4%, and 32.06% for these material pairs

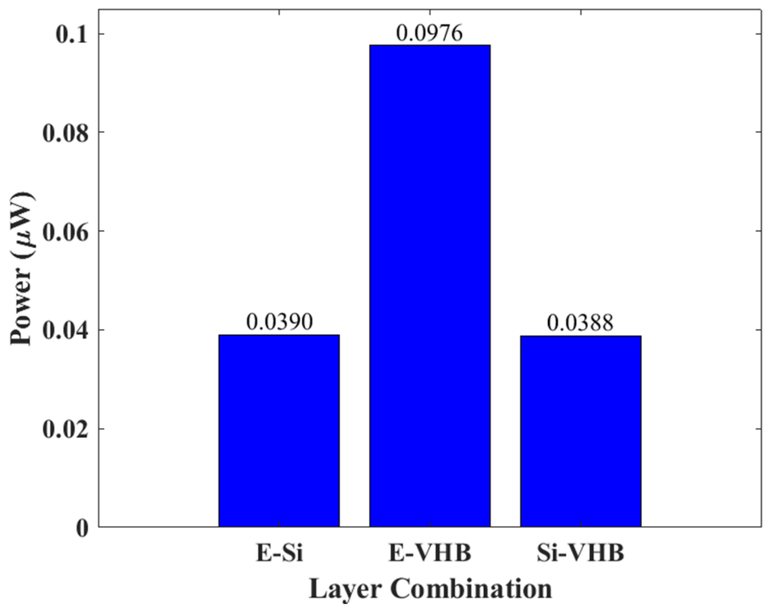

Figure 14. Output power of TENG in various layers combinations.

reflect these differences, predominantly influenced by varying mechanical properties impacting the overall efficiency of energy conversion. The efficiency of TENG can be further improved by reinforcing the various particle in base DE matrix to improve the dielectric constant [43–46]. All the studies have been carried out at atmospheric conditions, i.e., constant temperature of 298.15K, pressure of 1atm, however, the stability of the TENG can be affected by the materials ageing as it consists of elastomer layers, mechanical wear and fatigue, as well as the other change environmental conditions which will be focused in future investigation.

4. Conclusions

The present study highlights the potential of Triboelectric Nanogenerators (TENG) within the domain of green energy. TENG, as dielectric elastomer generators promises to extract energy from non-conventional sources, making it relevant in the search for sustainable energy solutions. TENG subjected to real-time vibrating energy conditions involves variation in both amplitude and frequency. The effects of varying frequency, at a consistent amplitude of 0.2mm, lead to an increment in velocity. At a higher frequency of 55 Hz, the output voltage increases can be attributed to the augmented release rate of energy, from higher velocity. It is essential to emphasize that output voltage is dependent on the relative permittivity of the TENG layers as well. Specifically, at a separation distance of 0.1mm, elastomer layers with low dielectric constant accumulated less voltage when compared to their counterparts possessing higher values. Furthermore, the separation distance exerted a considerable influence on voltage output, results indicate that increasing the separation distance in TENG led to enhanced voltage output. However, higher separation distances necessitate a source of energy with greater amplitude, which limits the application of TENG. The modified model holds the potential to aid researchers in the construction or adaptation of energy harvesters, specifically tailored to harness energy from low-frequency and low-amplitude vibrating sources.

Acknowledgments

The authors acknowledge the advanced material characterization lab of the Department of Mechanical Engineering for providing the necessary facilities.

Funding: The author (s) have not received any funding for the research work.

Author contributions: O. P. Prabhakar: Conceptualization, data curation, formal analysis, investigation, methodology, validation, visualization, writing- original draft. D. Sahu: Conceptualization, formal analysis, investigation, writing- original draft. R. K. Sahu: Supervision, validation, visualization, writing: review editing.

Disclosure statement: The authors declare no conflict of interest.

References

[1] Subhradeep Mandal, Mikhail Malanin, Bholanath Ghanti, Susanta Banerjee, Jun Sawada, Toshio Tada, Gert Heinrich, Sven Wießner, and Amit Das. Design of sacrificial network in modified natural rubber leads to strikingly improved mechanical performance with self-healing capability. *Chemical Engineering Journal*, 474:145838, October 2023.

[2] K A Cook-Chennault, N Thambi, and A M Sastry. Powering mems portable devices—a review of non-regenerative and regenerative power supply systems with special emphasis on piezoelectric energy harvesting systems. *Smart Materials and Structures*, 17(4):043001, June 2008.

[3] A. Erturk, W. G. R. Vieira, C. De Marqui, and D. J. Inman. On the energy harvesting potential of piezoaeroelastic systems. *Applied Physics Letters*, 96(18), May 2010.

[4] S P Beeby, R N Torah, M J Tudor, P Glynne-Jones, T O'Donnell, C R Saha, and S Roy. A micro electromagnetic generator for vibration energy harvesting. *Journal of Micromechanics and Microengineering*, 17(7):1257–1265, June 2007.

[5] Bin Yang, Chengkuo Lee, Wenfeng Xiang, Jin Xie, Johnny Han He, Rama Krishna Kotlanka, Siew Ping Low, and Hanhua Feng. Electromagnetic energy harvesting from vibrations of multiple frequencies. *Journal of Micromechanics and Microengineering*, 19(3):035001, January 2009.

[6] D. Peter, R. Pichler, S. Bauer, and R. Schwödiauer. Electrostatic converter with an electret-like elastomer membrane for large scale energy harvesting of low density energy sources. *Extreme Mechanics Letters*, 4:38–44, September 2015.

[7] Ron Pelrine, Roy D. Kornbluh, Joseph Eckerle, Philip Jeuck, Seajin Oh, Qibing Pei, and Scott Stanford. Dielectric elastomers: generator mode fundamentals and applications. In Yoseph Bar-Cohen, editor, *Smart Structures and Materials 2001: Electroactive Polymer Actuators and Devices*. SPIE, July 2001.

[8] Xiaofeng Wang, Simiao Niu, Yajiang Yin, Fang Yi, Zheng You, and Zhong Lin Wang. Triboelectric nanogenerator based on fully enclosed rolling spherical structure for harvesting low-frequency water wave energy. *Advanced Energy Materials*, 5(24), November 2015.

[9] Zuci Quan, Chang Bao Han, Tao Jiang, and Zhong Lin Wang. Wind energy: Robust thin films-based triboelectric nanogenerator arrays for harvesting bidirectional wind energy (adv. energy mater. 5/2016). *Advanced Energy Materials*, 6(5), March 2016.

[10] S. Chiba, M. Waki, T. Wada, Y. Hirakawa, K. Masuda, and T. Ikoma. Consistent ocean wave energy harvesting using electroactive polymer (dielectric elastomer) artificial muscle generators. *Applied Energy*, 104:497–502, April 2013.

[11] Hyung-Man Kim. Electroactive polymers for ocean kinetic energy harvesting: literature review and research needs. *Journal of Ocean Engineering and Marine Energy*, 4(4):343–365, October 2018.

[12] Seiki Chiba, Mikio Waki, Roy Kornbluh, and Ron Pelrine. Innovative wave power generation system using electroactive polymer artificial muscles. In *OCEANS 2009-EUROPE*, page 1–3. IEEE, May 2009.

[13] Roy D. Kornbluh, Ron Pelrine, Harsha Prahlad, Annjoe Wong-Foy, Brian McCoy, Susan Kim, Joseph Eckerle, and Tom Low. *From Boots to Buoys: Promises and Challenges of Dielectric Elastomer Energy Harvesting*, page 67–93. Springer US, 2012.

[14] Soo Jin Adrian Koh, Christoph Keplinger, Tiefeng Li, Siegfried Bauer, and Zhigang Suo. Dielectric elastomer generators: How much energy can be converted? *IEEE/ASME Transactions on Mechatronics*, 16(1):33–41, February 2011.

[15] Zhihui Lai, Shuaibo Wang, Likuan Zhu, Guoqing Zhang, Junlei Wang, Kai Yang, and Daniil Yurchenko. A hybrid piezo-dielectric wind energy harvester for high-performance vortex-induced vibration energy harvesting. *Mechanical Systems and Signal Processing*, 150:107212, March 2021.

[16] Om Prakash Prabhakar and Raj Kumar Sahu. Effect of filler on anisotropic behavior of dielectric elastomer composite. *Materials Today: Proceedings*, 44:3172–3176, 2021.

[17] Giacomo Moretti, Gastone Pietro Rosati Papini, Michele Righi, David Forehand, David Ingram, Rocco Vertechy, and Marco Fontana. Resonant wave energy harvester based on dielectric elastomer generator. *Smart Materials and Structures*, 27(3):035015, February 2018.

[18] Xuan Yuan, Shuai Changgeng, Gao Yan, and Zhao Zhenghong. Application review of dielectric electroactive polymers (deaps) and piezoelectric materials for vibration energy harvesting. *Journal of Physics: Conference Series*, 744:012077, September 2016.

[19] C.L. Zhang, Z.H. Lai, X.X. Rao, J.W. Zhang, and D. Yurchenko. Energy harvesting from a novel contact-type dielectric elastomer generator. *Energy Conversion and Management*, 205:112351, February 2020.

[20] Yongyun Mao, Yong Li, Jiyang Xie, Huan Liu, Changjin Guo, and Wanbiao Hu. Triboelectric nanogenerator/supercapacitor in-one self-powered textile based on ptfe yarn wrapped pdms/mno2nw hybrid elastomer. *Nano Energy*, 84:105918, June 2021.

[21] Azad Kumar, Sumit Kumar, Arpit Kumar Pathak, Anees A. Ansari, R.N. Rai, Youngil Lee, Soo Young Kim, Quyet Van Le, and Laxman Singh. Recent progress in nanocomposite-oriented triboelectric and piezoelectric energy generators: An overview. *Nano-Structures amp; Nano-Objects*, 36:101046, October 2023.

[22] Kwi-Il Park, Chang Kyu Jeong, Na Kyung Kim, and Keon Jae Lee. Stretchable piezoelectric nanocomposite generator. *Nano Convergence*, 3(1), June 2016.

[23] Yang Wang, Ya Yang, and Zhong Lin Wang. Triboelectric nanogenerators as flexible power sources. *npj Flexible Electronics*, 1(1), November 2017.

[24] Kamal Kumar Meena, Injamamul Arief, Anik Kumar Ghosh, Hans Liebscher, Sakrit Hait, Jürgen Nagel, Gert Heinrich, Andreas Fery, and Amit Das. 3d-printed stretchable hybrid piezoelectric-triboelectric nanogenerator for smart tire: Onboard real-time tread wear monitoring system. *Nano Energy*, 115:108707, October 2023.

[25] Wittawat Thongthapthai, Viyada Harnchana, Chalathorn Chanthad, Vittaya Amornkitbamrung, and Prinya Chindaprasirt. The fabrication of calcium silicate-natural rubber composite for mechanical energy harvesting. *Surfaces and Interfaces*, 25:101180, August 2021.

[26] Renjie Xu, Lifeng Zhu, Qirui Zhang, Zijian Wang, Lanyue Shen, Yunfeng Chen, Hao Lei, Xiangchao Ge, Jinxing Jiang, Jingya Liu, Yanyun Ma, Xuhui Sun, and Zhen Wen. Laminated triboelectric nanogenerator for enhanced self-powered pressure-sensing performance by charge regulation. *ACS Applied Materials amp; Interfaces*, 14(35):40014–40020, August 2022.

[27] Ede Mehta Wardhana, Hidemi Mutsuda, Yoshikazu Tanaka, Takuji Nakashima, Taiga Kanehira, Naokazu Taniguchi, Shuhei Maeda, Takayuki Yonezawa, and Masaaki Yamauchi. Harvesting contact-separation-compression vibrations using a flexible and compressible triboelectric generator. *Sustainable Energy Technologies and Assessments*, 42:100869, December 2020.

[28] Zhong Lin Wang and Jinhui Song. Piezoelectric nanogenerators based on zinc oxide nanowire arrays. *Science*, 312(5771):242–246, April 2006.

[29] Moonkang Choi, Gonzalo Murillo, Sungmin Hwang, Jae Woong Kim, Jong Hoon Jung, Chih-Yen Chen, and Minbaek Lee. Mechanical and electrical characterization of pvdf-zno hybrid structure for application to nanogenerator. *Nano Energy*, 33:462–468, March 2017.

[30] Chieh Chang, Van H. Tran, Junbo Wang, Yiin-Kuen Fuh, and Liwei Lin. Direct-write piezoelectric polymeric nanogenerator with high energy conversion efficiency. *Nano Letters*, 10(2):726–731, January 2010.

[31] Zhong Lin Wang, Jun Chen, and Long Lin. Progress in triboelectric nanogenerators as a new energy technology and self-powered sensors. *Energy Environmental Science*, 8(8):2250–2282, 2015.

[32] Swayam Aryam Behera, Hang-Gyeom Kim, Il Ryu Jang, Sugato Hajra, Swati Panda, Naratip Vittayakorn, Hoe Joon Kim, and P. Ganga Raju Achary. Triboelectric nanogenerator for self-powered traffic monitoring. *Materials Science and Engineering: B*, 303:117277, May 2024.

[33] C. Generator. Application guidance notes: Technical information. https://www.stamford-avk.com/sites/stamfordavk/files/AGN008_C.pdf, 2006. [Online]. Available: Accessed on: Feb. 11, 2025.

[34] O. P. Prabhakar and R. K. Sahu. Effect of strain induced variation in dielectric constant on performance of dielectric elastomer based cylindrical actuator. Technical report, National Institute of Technology Raipur, CG, India, 2019.

[35] Anjaly Babu, Lakshakoti Bochu, Supraja Potu, Ruthvik Kaja, Navaneeth Madathil, Mahesh Velpula, Anu Kulandaivel, Uday Kumar Khanapuram, Rakesh Kumar Rajaboina, Haranath Divi, Prakash Kodali, Balaji Ketharachapalli, and Rajanikanth Ammanabrolu. Facile direct growth of zif-67 metal–organic framework for triboelectric nanogenerators and their application in the internet of vehicles. *ACS Sustainable Chemistry amp; Engineering*, 11(47):16806–16817, November 2023.

[36] Sugato Hajra, Manisha Sahu, Aneeta Manjari Padhan, In Sang Lee, Dong Kee Yi, Perumal Alagarsamy, Sitansu Sekhar Nanda, and Hoe Joon Kim. A green metal–organic framework-cyclodextrin mof: A novel multifunctional material based triboelectric nanogenerator for highly efficient mechanical energy harvesting. *Advanced Functional Materials*, 31(28), April 2021.

[37] Anas A. Ahmed, Hasan M. Abdullah, Talal F. Qahtan, Asan G.A. Muthalif, Marwan Nafea, and Mohamed Sultan Mohamed Ali. An enhanced distance-dependent electric field model for contact-separation triboelectric nanogenerator: Air-breakdown limit as a case study. *Nano Energy*, 117:108836, December 2023.

[38] Ahmed Haroun and Chengkuo Lee. Dielectric-elastomer-enhanced triboelectric nanogenerator with amplified outputs. *Sensors and Actuators A: Physical*, 333:113270, January 2022.

[39] Raj Kumar Sahu and Karali Patra. Rate-dependent mechanical behavior of vhb 4910 elastomer. *Mechanics of Advanced Materials and Structures*, 23(2):170–179, October 2015.

[40] Om Prakash Prabhakar and Raj Kumar Sahu. Effects of soft and hard fillers on electromechanical properties and performance of polydimethylsiloxane elastomer for actuator applications. February 2023.

[41] Markus Mehnert, Jessica Faber, Mokarram Hossain, Shawn A. Chester, and Paul Steinmann. Experimental and numerical investigation of the electro-mechanical response of particle filled elastomers - part i: Experimental investigations. *European Journal of Mechanics - A/Solids*, 96:104651, November 2022.

[42] Shiva Sundar Yadava, Ankur Khare, Pooja Gautam, Laxman Singh, Youngil Lee, and K. D. Mandal. Dielectric, ferroelectric and magnetic properties of hexagonal ba6y2ti4o17 (byto) perovskite derived from semi wet route. *RSC Advances*, 6(106):104941–104948, 2016.

[43] Laxman Singh, Muhammad Sheeraz, Mahmudun Nabi Chowdhury, U. S. Rai, Shiva Sunder Yadava, Young Seok Park, Satya Vir Singh, and Youngil Lee. Investigation of dielectric, mechanical, and electrical properties of flame synthesized y2/3cu2.90zn0.10ti4o12 material. *Journal of Materials Science: Materials in Electronics*, 29(12):10082–10091, April 2018.

[44] Laxman Singh, Lokeswararao Dhavala, Rajasekhar Bhimireddi, Anees A. Ansari, Sunil Kumar, Vandana Srivastava, R.N. Rai, Quyet Van Le, and Youngil Lee. Low-cost flame synthesized la2/3cu3ti4o12 electro-ceramic and extensive investigation on electrical, impedance, modulus, and optical properties. *Ceramics International*, 49(13):21795–21803, July 2023.

[45] Laxman Singh, Ill Won Kim, Byung Cheol Sin, Sang Kook Woo, Seung Ho Hyun, Kam Deo Mandal, and Youngil Lee. Combustion synthesis of nano-crystalline bi2/3cu3ti2.90fe0.10o12 using inexpensive tio2 raw material and its dielectric characterization. *Powder Technology*, 280:256–265, August 2015.

[46] Laxman Singh, Shiv Sunder Yadava, Won Seok Woo, Uma Shanker Rai, K. D. Mandal, Byung Cheol Sin, and Youngil Lee. Structural, impedance, and modulus spectroscopic studies on y2/3cu3ti3.95in0.05o12polycrystalline material prepared by flame synthesis method. *Applied Spectroscopy Reviews*, 51(7–9):735–752, March 2016.